



Asymmetry and Variability in the Transmission Spectra of Tidally Locked Habitable Planets

Xinyi Song and Jun Yang*

Department of Atmospheric and Oceanic Sciences, School of Physics, Peking University, Beijing, China

OPEN ACCESS

Edited by:

Hans J. Deeg,
Instituto de Astrofísica de Canarias,
Spain

Reviewed by:

Antigona Segura,
National Autonomous University of
Mexico, Mexico
Mark Hammond,
University of Bristol, United Kingdom

*Correspondence:

Jun Yang
junyang@pku.edu.cn

Specialty section:

This article was submitted to
Exoplanets,
a section of the journal
Frontiers in Astronomy and Space
Sciences

Received: 11 May 2021

Accepted: 29 July 2021

Published: 22 September 2021

Citation:

Song X and Yang J (2021) Asymmetry
and Variability in the Transmission
Spectra of Tidally Locked
Habitable Planets.
Front. Astron. Space Sci. 8:708023.
doi: 10.3389/fspas.2021.708023

Spatial heterogeneity and temporal variability are general features in planetary weather and climate, due to the effects of planetary rotation, uneven stellar flux distribution, fluid motion instability, etc. In this study, we investigate the asymmetry and variability in the transmission spectra of 1:1 spin-orbit tidally locked (or called synchronously rotating) planets around low-mass stars. We find that for rapidly rotating planets, the transit atmospheric thickness of the evening terminator (east of the substellar region) is significantly larger than that of the morning terminator (west of the substellar region). The asymmetry is mainly related to the spatial heterogeneity in ice clouds, as the contributions of liquid clouds and water vapor are smaller. The underlying mechanism is that there are always more ice clouds on the evening terminator, due to the combined effect of coupled Rossby–Kelvin waves and equatorial superrotation that advect vapor and clouds to the east, especially at high levels of the atmosphere. For slowly rotating planets, the asymmetry reverses (the morning terminator has a larger transmission depth than the evening terminator), but the magnitude is small or even negligible. For both rapidly and slowly rotating planets, there is strong variability in the transmission spectra. The asymmetry signal is nearly impossible to be observed by the James Webb Space Telescope (JWST), because the magnitude of the asymmetry (about 10 ppm) is smaller than the instrumental noise and the high variability further increases the challenge.

Keywords: transit spectroscopy, exoplanet atmospheres, asymmetry, variability, superrotation, tidally locked planets

1 INTRODUCTION

More than 4,600 exoplanets have been discovered since the discovery of 51 Pegasi b in 1995 (Mayor and Queloz, 1995), with an ever-growing fraction of terrestrial planets that are smaller than Neptune and Uranus. Astronomers are now at the stage of characterizing atmospheric compositions of rocky planets. Transmission spectrum, emission spectrum, and reflection spectrum are three of the main methods used for atmospheric characterizations (Seager and Sasselov, 2000; Hubbard et al., 2001; Charbonneau et al., 2002; Deming and Seager, 2017; Kaltenegger, 2017; Kreidberg, 2017; de Wit et al., 2018; Grimm et al., 2018; Schwieterman et al., 2018). In this study, we focus on the transmission spectrum. Stellar light is absorbed and scattered by atmospheric species when traveling through the planetary limb; therefore, at wavelengths where the molecules in the atmosphere have higher opacity, the planet will block more light from the star, having a higher relative transit depth. The upcoming launch of telescopes such as the JWST may enable us to detect transmission spectra with higher resolution, larger spectral coverage, and longer observing duration, which will be a breakthrough in this area, especially for Earth-sized planets.

Transmission spectroscopy is useful and effective in detecting atmospheric compositions of hot Jupiters, and even hot sub-Neptunes and super-Earths (Sing et al., 2011; Nikolov et al., 2014; Wakeford and Sing, 2015; Benneke et al., 2019; Iyer and Line, 2020; Mikal-Evans et al., 2020). However, the present telescopes are not able to resolve the atmospheric spectra of habitable terrestrial planets that are smaller in size and cooler in temperature. Theoretical analyses and numerical simulations showed that atmospheric CO₂ at 4.3 μm on tidally locked planets is detectable by the JWST, but not for other molecular signatures, such as H₂O, because clouds (as well as haze) strongly mute the spectral features (Snellen et al., 2017; Lincowski et al., 2018; Fauchez T. J. et al., 2019; Komacek and Abbot, 2019; Lustig-Yaeger et al., 2019; Suissa et al., 2020a; Lacy and Burrows, 2020; Pidhorodetska et al., 2020). Clouds cause a 10–100-time increase in the transit number required to detect H₂O using the JWST (Komacek and Abbot, 2019). Due to convection and large-scale circulation, the dayside of tidally locked habitable planets should be covered by clouds, especially over the substellar region (Yang et al., 2013, 2019a; Haqq-Misra et al., 2018; Fauchez T. J. et al., 2019; Komacek and Abbot, 2019; Suissa et al., 2020a).

In estimating the transmission spectra of tidally locked planets, previous studies (Fauchez T. J. et al., 2019; Komacek et al., 2020; Suissa et al., 2020a) have calculated the average of the two terminators, assuming the differences between the morning terminator and the evening terminator are small or negligible. However, this assumption is groundless. Due to the single-direction rotation of the planet (clockwise or counterclockwise) and flow motion instability, asymmetry is unavoidable even for an aqua-planet with an ocean covering the whole surface. The atmospheric circulation on tidally locked planets is characterized by coupled Rossby–Kelvin waves and equatorial superrotation (Showman and Polvani, 2010, 2011; Koppapapu et al., 2016; Haqq-Misra et al., 2018). Rossby–Kelvin waves and equatorial superrotation are able to advect heat, clouds, and species (such as H₂O) to the east of the substellar point and can induce spatial asymmetry. We find that the asymmetry in the transmission spectra between the two terminators is significant and is comparable to the molecular signatures of H₂O in magnitude (see **section 3** below).

The feature of significant asymmetry in transmission spectra has already been found in the observations and simulations of hot exoplanets (Dobbs-Dixon et al., 2012; Line and Parmentier, 2016; von Paris et al., 2016; Parmentier et al., 2018; Powell et al., 2019; Ehrenreich et al., 2020; Lacy and Burrows, 2020; Pluriel et al., 2020; Kesseli and Snellen, 2021), but not for cool, habitable terrestrial planets. For example, an asymmetric feature in iron absorption of the hot Jupiter WASP-76b was confirmed by the High Accuracy Radial velocity Planet Searcher (HARPS) (Ehrenreich et al., 2020; Kesseli and Snellen, 2021). The asymmetry is always caused by nonuniform cloud coverage (Line and Parmentier, 2016), which in turn is largely determined by thermal contrasts and atmospheric dynamics.

Another feature that was always ignored in the previous studies of terrestrial planets (Lincowski et al., 2018; Lustig-Yaeger et al., 2019; Fauchez T. J. et al., 2019; Komacek and Abbot, 2019; Lacy and Burrows, 2020; Pidhorodetska et al., 2020; Suissa et al., 2020a,b) is the variability of the transmission spectra.

On account of waves and fluid motion instabilities, there may be strong short-term variability in the atmosphere although there is neither a seasonal cycle nor a diurnal cycle on the 1:1 tidally locked planets. The variability is unimportant for the mean climate, but it is critical for atmospheric characterizations. This is because a strong (weak) variability implies that more (less) observation time is required for resolving the molecular signals or the asymmetry properly. Previous studies on brown dwarfs and sub-Neptunes (such as Artigau et al., 2009; Radigan et al., 2012; Apai et al., 2013; Showman et al., 2013, 2019; Charnay et al., 2021) have found that the cloud fraction at the terminators could be highly variable.

Recent model calculations by May et al. (2021) show that variability of patchy ice cloud is present in the upper atmospheres of M-dwarf terrestrial planets, particularly along the limbs. However, their study still uses the same method as previous studies, assuming the differences between the morning terminator and the evening terminator are small or negligible, and calculates the average of the two terminators. Here in our study, we examine the asymmetry in the transmission spectra between the morning terminator and the evening terminator, and the variability of this asymmetry. Moreover, while May et al. (2021) examined only one rapidly rotating planet TRAPPIST-1e, our study examines the results of both rapidly and slowly rotating planets. Note that in order to have habitable environments permitting the existence of liquid water, a planet has to be rather close to an M-dwarf, such as 0.1 AU, since M-dwarfs are relatively cool and dim. Such a small orbit would result in a significant gravity gradient along the planet's diameter. The gravitational pull on the planet can lead to torques that force the planet to synchronize its rotation period with its orbital period. The time scale for the evolution of one habitable planet from asynchronous rotation to synchronous rotation depends on many factors, such as the orbital distance, stellar mass, the energy dissipation rate, the rigidity of the planet, the initial planetary rotation rate, land-sea configuration, and ocean bottom topography (Kasting et al., 1993; Barnes, 2017; Pierrehumbert and Hammond, 2019). Habitable planets around low-mass stars are more likely to be in a synchronous rotation than Earth.

To calculate the asymmetry and variability between morning and evening terminators in transmission spectra of tidally locked terrestrial planets, we post-process 3D climatic outputs of the atmospheric general circulation model (AGCM) in Zhang and Yang (2020) to calculate JWST observations of transmission spectra for morning and evening terminators, respectively. In **section 2**, we describe the settings for the AGCM experiments and how we post-process the AGCM results to obtain the transmission spectra and its variability. Then, we present the transmission spectra and estimate the number of transits required to detect this asymmetry signal in **section 3**. A summary is given in **section 4**.

2 METHODS

2.1 Simulation of the Climate

We employed the three-dimensional (3D) atmospheric general circulation model (AGCM) ExoCAM in our climate simulations (Zhang and Yang, 2020). ExoCAM was developed based on the

Community Atmosphere Model version 4 but with correlated k radiative transfer and had updated water vapor continuum absorption coefficients from HITRAN 2012 (Wolf and Toon, 2014; Wolf, 2017; Wolf et al., 2017). In the experiments, planetary radius, gravity, and atmospheric conditions are the same as Earth, except we only include N_2 and H_2O . The atmosphere is coupled to a 50-m immobile slab ocean with no oceanic heat transport and no continent. The horizontal resolution is 4° by 5° (46 grid points in latitude and 72 grid points in longitude). The model has 40 layers vertically, with surface pressure of 1 bar and a model top of 1 hPa. The stellar flux is 1350 W m^{-2} , and the stellar spectra are from the BT_Settl stellar model (Allard et al., 2007). The stellar temperature is 2600 K for the rapidly rotating planet and 3700 K for the slowly rotating planet.

Since the simulations presented in this study are non-runaway planets, which mean their cloud deck lies well below the original model top, there is no need to extend the layers of the atmospheric profiles (Suissa et al., 2020a). The results of two cases, with rotation periods of 6 and 60 Earth days, are shown in the main text, as they are the most representative ones. Results of other experiments with different surface pressures and stellar fluxes are discussed at the end of the study. The experiments are set to be 1:1 tidally locked (rotation period = orbital period). Each of the experiments was run for tens of Earth years. We use the 365 daily outputs of the last year of the experiments to analyze the transmission spectra and their viability.

Our experimental design is different from that of Kopparapu et al. (2016) and Kopparapu et al. (2017), who modified the rotation period and the stellar flux simultaneously in their experiments, self-consistently considering the effect of the Coriolis force and stellar flux as a whole instead of two standalone factors. We use the same method as Merlis and Schneider (2010), Way et al. (2016), Noda et al. (2017), and Bin et al. (2018), with the rotation period fixed when varying the stellar flux or with the stellar flux fixed when varying the rotation period. This method allows us to know the separate effects of varying the rotation period and varying the stellar flux. The combined effect of varying the rotation period and the stellar flux needs future studies.

2.2 Calculation of the Transmission Spectra

We use the Planetary Spectrum Generator¹ (PSG, Villanueva et al., 2018) to calculate the transmission spectra. The method used here is similar to that used in Fauchez T. J. et al. (2019), Suissa et al. (2020a), and Komacek et al. (2020). They averaged transmission spectra of the two terminators, but we calculate transmission spectra for the morning terminator and the evening terminator, respectively. In theory, the transmission spectra of the morning terminator can be obtained during the ingress, and the transmission spectra of the evening terminator can be obtained during the egress, as shown in **Figure 1**. In practice, the process for obtaining the separate morning and evening spectra is more complex; please refer to the study by Espinoza and Jones (2021). What is more, unlike previous studies (such as Komacek et al., 2020) that use the climatology outputs averaged over the last

10 years of the simulation time, we use the daily output of the experiments, so our analyses are able to resolve the variability of the spectra. We use PSG to calculate the transmission spectrum for every model grid point along the terminator, and then average the spectra with equal weighting of each grid.

We calculate the transmission spectra with a resolving power (R) of 300, from 0.6 to $5 \mu\text{m}$, within the range of the near infrared spectrograph instrument (NIRSpec) on the JWST, and it has been shown that NIRSpec is the best instrument for JWST characterization of terrestrial exoplanets (Batalha et al., 2018; Lincowski et al., 2019; Lustig-Yaeger et al., 2019). Since we do not include a noise floor and only use the PSG imager noise model in the calculations, the estimated results for the number of required transits to detect the spectral features should be considered as a lower limit. We set the output of PSG in the form of relative transit atmospheric thickness. The relative transit depth can be calculated by the following mathematical expression (Winn, 2010):

$$\delta\Delta = (\delta R/R_s)^2 + (2 \times R_p \times \delta R)/R_s^2 \approx (2 \times R_p \times \delta R)/R_s^2, \quad (1)$$

with R_p , δR , and R_s the planet's radius, transit atmospheric thickness, and the radius of the star, respectively. Δ is the transit depth, and $\delta\Delta$ is the relative transit depth. Note that during the following calculations, we assume that the rapidly rotating case and the slowly rotating case have the same stellar radius as TRAPPIST-1 (0.12 solar radius), and the planet radius is the same as TRAPPIST-1e (0.91 Earth's radius). The influence of stellar radius is further discussed in **section 4**.

3 RESULTS

3.1 Asymmetry in the Transmission Spectra

Figure 2A shows the transmission spectra for one tidally locked aqua-planet with a rotation period of six Earth days. It is clear that the transit atmospheric thickness of the morning terminator (west of the substellar point, red line) is in general smaller than that of the evening terminator (east of the substellar point, blue line) in every wavelength. The magnitude of the differences between these two lines is in the order of 10 ppm (**Figure 2C**). This magnitude is comparable to the molecular absorption signals of H_2O , such as the signal at $1.4 \mu\text{m}$. In this figure, all of the absorption features are due to water vapor and clouds, except for the $4.3 \mu\text{m}$ feature caused by N_2 - N_2 collision-induced absorption.

To determine which factor is the main cause of the asymmetry between morning and evening terminators, we calculated the contributions of air temperature, water vapor, liquid clouds, and ice clouds, respectively, as shown in **Figures 2E,F**. When calculating the contribution of liquid clouds, for example, we set temperature, water vapor, and ice clouds with the same values on both morning and evening terminators. It turns out that ice clouds contribute the most to the differences, while the contributions of the asymmetry in air temperature, water vapor, and liquid clouds are much smaller. This is due to the fact that ice clouds are in the high-altitude levels where the optical thicknesses of water vapor and liquid clouds are relatively smaller, thereby they have stronger influence on the transit depth.

¹<https://psg.gsfc.nasa.gov>

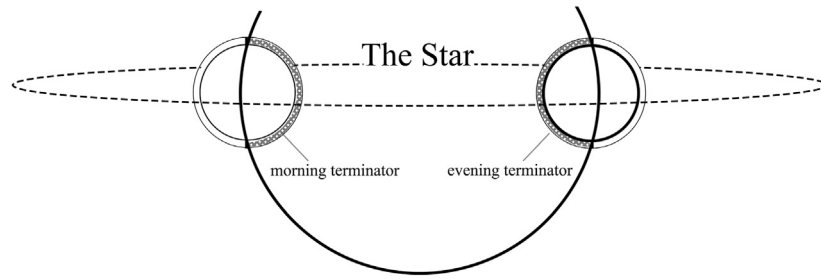


FIGURE 1 | The orbital geometry of a transiting exoplanet system. The dashed line is the planetary orbit, the thick solid line is the edge of the star, and two phases of the planet during the ingress and egress are shown. The asymmetry between the transit depth of the morning terminator during the ingress and the transit depth of the evening terminator during the egress leads to a distorted light curve.

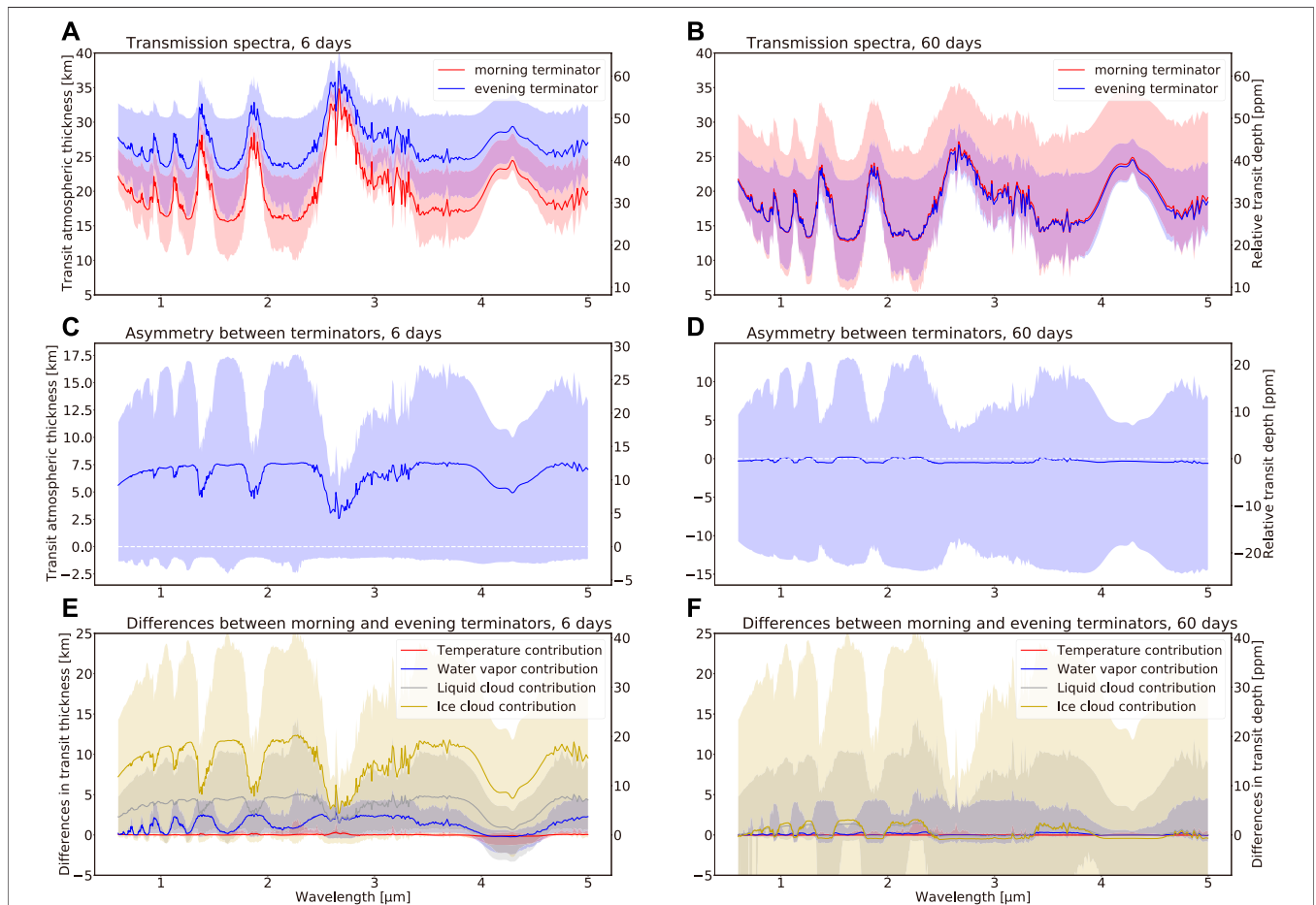
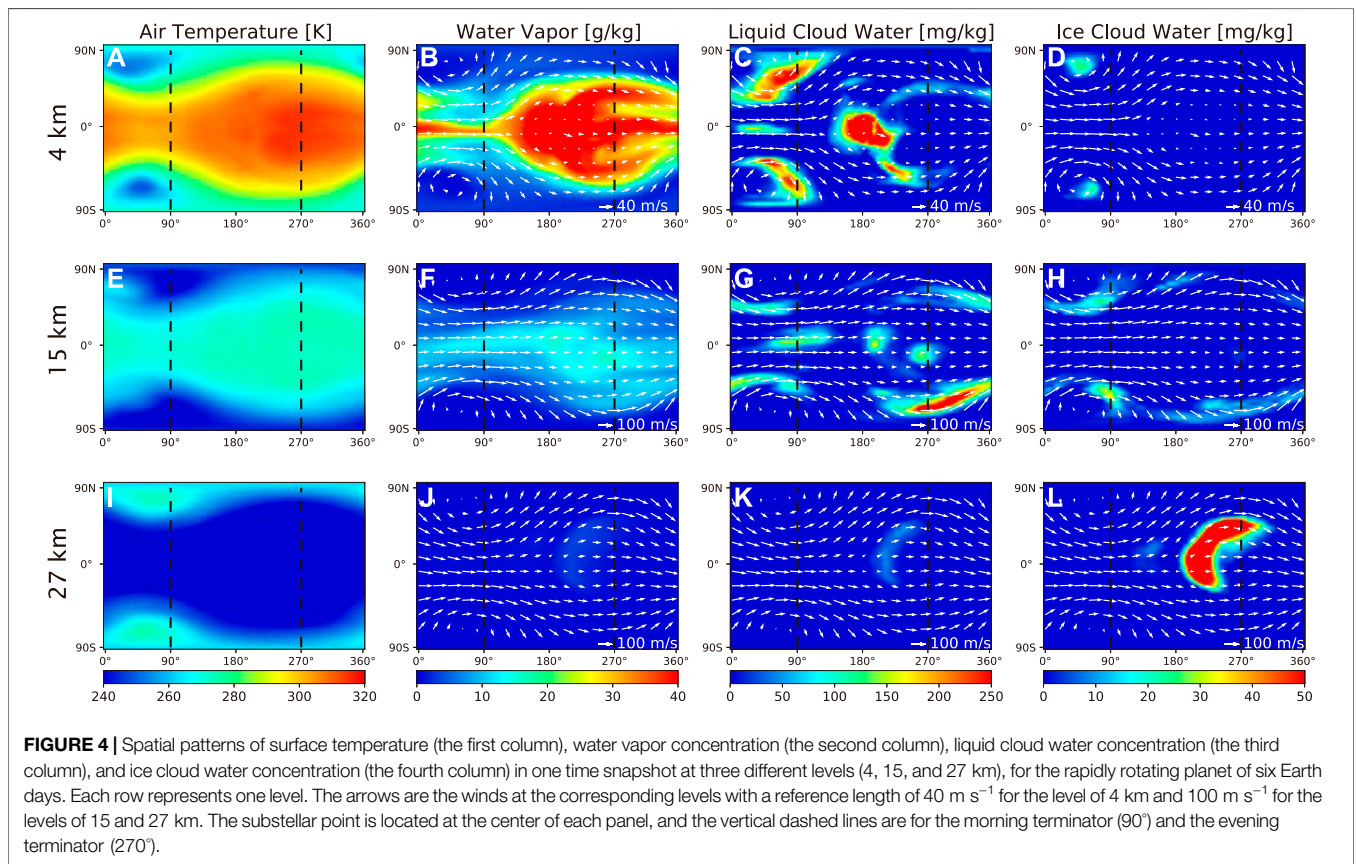
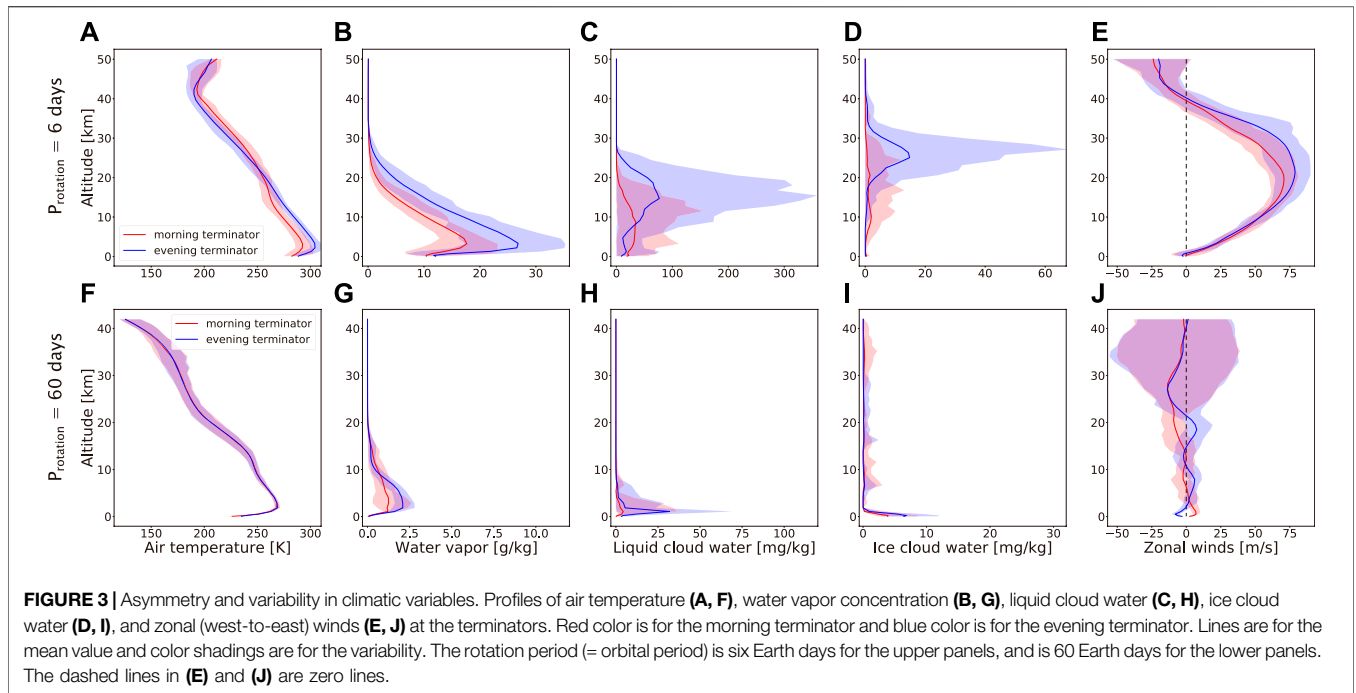
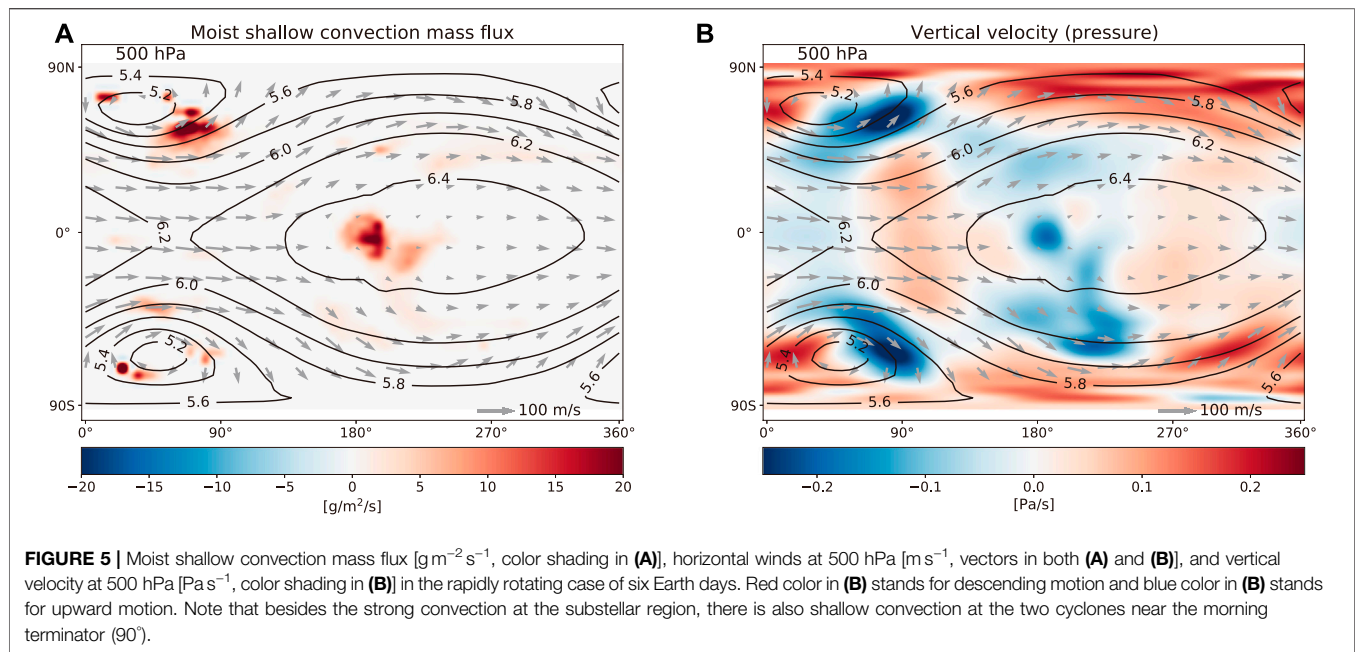


FIGURE 2 | Transmission spectra and their variability of tidally locked planets, from 0.6 to 5 μm. The left y-axis is the transit atmospheric thickness (km) and the right y-axis is the relative transit depth (ppm). **(A)**, **(C)**, and **(E)**: results for planets with a rotation period of six Earth days (= orbital period); **(B)**, **(D)**, and **(F)**: for planets with a rotation period of 60 Earth days. In **(A)** and **(B)**, the blue line is for the evening terminator and the red line is for the morning terminator, and the areas shaded with pale blue and pale red show their variability. In **(C)** and **(D)**, the blue line is for the average value of the asymmetry (evening minus morning), and the areas shaded with pale blue show their variability. In **(E)** and **(F)**, the contributions of air temperature, water vapor, liquid clouds, and ice clouds to the asymmetry (evening minus morning) are shown in red, blue, gray, and yellow, respectively, and their variability are shaded with the corresponding pale colors. The surface pressure is 1 bar, including only N₂ and H₂O. Note that the summary of the four lines in the lower panel [such as **(E)**] is not exactly equal to the difference between the blue line and the red line in the upper panel [such as **(A)**]; this is mainly due to the overlaps among water vapor, liquid clouds, and ice clouds.





Water vapor concentration at the evening terminator is greater than that at the morning terminator in every layer (**Figure 3B**). This is caused by atmospheric superrotation and coupled Kelvin–Rossby waves (excited from the uneven distribution of stellar flux; Showman and Polvani (2010, 2011); Tsai et al. (2014); Hammond and Pierrehumbert (2018); Pierrehumbert and Hammond (2019); Wang and Yang (2021)), which advects low-concentration water vapor from the nightside to the west terminator and meanwhile advects high-concentration water vapor from the substellar region to the east of the substellar point, as shown in **Figures 4B,F,J**.

The vertical distributions of the liquid cloud water path and the ice cloud water path (**Figures 3C,D**) are more complex. For ice clouds, the concentration below the level of ≈ 20 km at the morning terminator is larger than that at the evening terminator, but above that level, the contrast reverses and the evening terminator has more ice clouds than the morning terminator. The liquid cloud concentration distribution is similar to that of ice cloud, but for liquid clouds the reverse occurs at a lower level of ≈ 10 km.

Detailed analyses find that clouds (both liquid and ice) at the morning terminator mainly form at the local region, whereas clouds at the evening terminator are mainly advected from the substellar region by horizontal winds (**Figure 4**). There are two key regions where clouds form: one well-known region is the substellar area and the other barely known one is the cyclone region (characterized by low pressure, anticlockwise winds in the northern hemisphere and clockwise winds in the southern hemisphere, and upwelling motion) near the morning terminator, as shown in **Figure 5**. Therefore, at low levels of the atmosphere, the morning terminator has more liquid and ice clouds than the evening terminator. At high levels (such as ≥ 20 km for ice clouds), the morning terminator has less ice clouds than the evening terminator; this is because the zonal westerly winds transport clouds from the substellar region to the east terminator (**Figure 4L**). Note that the

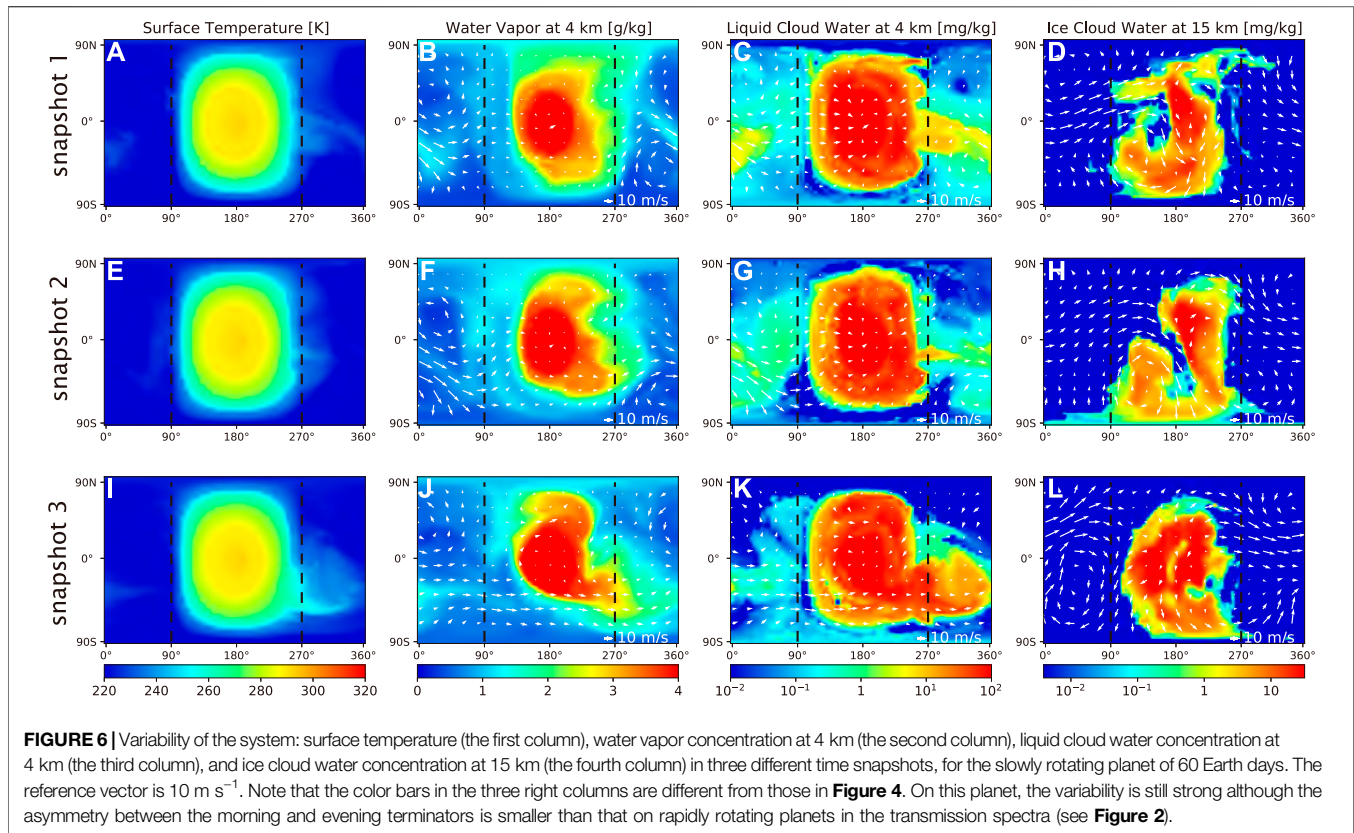
zonal winds at high-altitude (above ≈ 10 km) are enhanced, so the eastward transport of clouds to the evening terminator is not significant below the level of ≈ 10 km for liquid clouds and below the level of ≈ 20 km for ice clouds.

For a slowly rotating planet of 60 Earth days, the asymmetry is much smaller than that of the rapidly rotating one (**Figure 2D, C**). This is reasonable because as the rotation period increases, the baroclinic instability and the interaction between waves and mean flow become weaker (Vallis, 2017) so that the climatic variables of the slowly rotating planet (such as air temperature, water vapor, liquid clouds, and ice clouds shown in **Figures 3F–I**) are much more symmetric between the two terminators, compared with those of the rapidly rotating planet (**Figures 3A–E**). Imagining a planet with no rotation and with uniform boundary conditions (such as the aqua-planet employed here), the asymmetry may be close to zero.

Interestingly, the transit atmospheric thickness of the morning terminator is slightly larger than that of the evening terminator in the slowly rotating case; it is opposite to the result of the rapidly rotating case. This is due to the fact that the strength of atmospheric superrotation is much weaker in the slowly rotating case than in the rapidly rotating case (**Figure 3J, E**, same as that found in Kopparapu et al. (2016, 2017); Haqq-Misra et al. (2018)). Thus, horizontal advection has nearly no effect on the cloud concentration at the east (evening) terminator, whereas the west (morning) terminator, where clouds form locally, can have more clouds (such as at the levels above 30 km, shown in **Figure 3I**) and a larger transit depth (see **Figure 2B**) than the east terminator.

3.2 Strong Variability in the Transmission Spectra

Besides the asymmetry, there is also strong variability in the transmission spectra, as the color shading showed in **Figure 2**.



The amplitude of the variability is in the order of 20 ppm, larger than the asymmetry and H_2O signals. The variability in the transmission spectra is caused by the strong variability in water vapor, liquid clouds, and ice clouds, especially the latter, as shown in **Figures 3, 6**. For slowly rotating planets, the variability in the transmission spectra is comparable to that of the rapidly rotating planets, because the vortices on slowly rotating planets move more freely (**Figure 6**), while those in the rapidly rotating case are confined to the region near the morning terminator. Although the spatial pattern of the surface temperature is relatively stable (left panels in **Figure 6**), all of the waves, barotropic instability, baroclinic instability, and the interaction between the waves and the mean flow are able to induce oscillations and randomness in the system. We tried the Fourier analysis on the time series of transit atmospheric thickness and climate variables, but we did not find any notable period. The strong variability and irregularity make the asymmetry signal nearly impossible to be observed.

Note that the variability in climate variables (air temperature, water vapor amount, and liquid and ice cloud water contents) of the rapidly rotating planet is much larger than that of the slowly rotating planet (**Figure 3**), but the variability in the transmission spectra is comparable between the slowly and rapidly rotating planets, as shown in **Figure 2**. This is due to a “saturation” effect: when the content of a climate variable, such as ice cloud water content, reaches a certain value, the optical depth will be far greater than one, so that the increment of the climate variable content will not

significantly increase the atmospheric opacity; thus the transit atmospheric thickness remains almost the same. To explain this phenomenon, we varied the maximum value of ice cloud water profile for every grid along the terminator of a rapidly rotating planet. The results are shown in **Figure 7**. When ice cloud water content exceeds 7 mg kg^{-1} , it becomes “saturated”, and the transit atmospheric thickness is almost the same as the original. Although the variability in climate variables of the rapidly rotating planet is rather large (**Figures 3A–E**), they are confined to low altitudes and are “saturated”, so they will not contribute much to the variability. The amplitude of the variability depends mostly on the amount of ice cloud and water at high altitudes that are not “saturated”.

We calculate the number of transits required to reach a given signal-to-noise (SNR) ratio, assuming that the overall SNR is in proportion to the square root of the number of transit events, and is also in proportion to the SNR for one transit, following the method used in *Lustig-Yaeger et al. (2019)*. Approximately, for a planet with a rotation period of six Earth days, it requires 19 transits to achieve 3σ detection and 53 transits to achieve 5σ detection. The nominal lifetime of the JWST is 5 years. If 30% of the observation time is given to exoplanets, the possible maximum number of transits for an orbital period of 6 days is ≈ 90 . Unlike the detection of molecular signatures, which are restricted to their absorption lines, the asymmetry signal exists in broad band-pass, so there is not much variation in the required number of transits for different wavelengths, except for several particular absorption lines. For a planet with a 60-day rotation

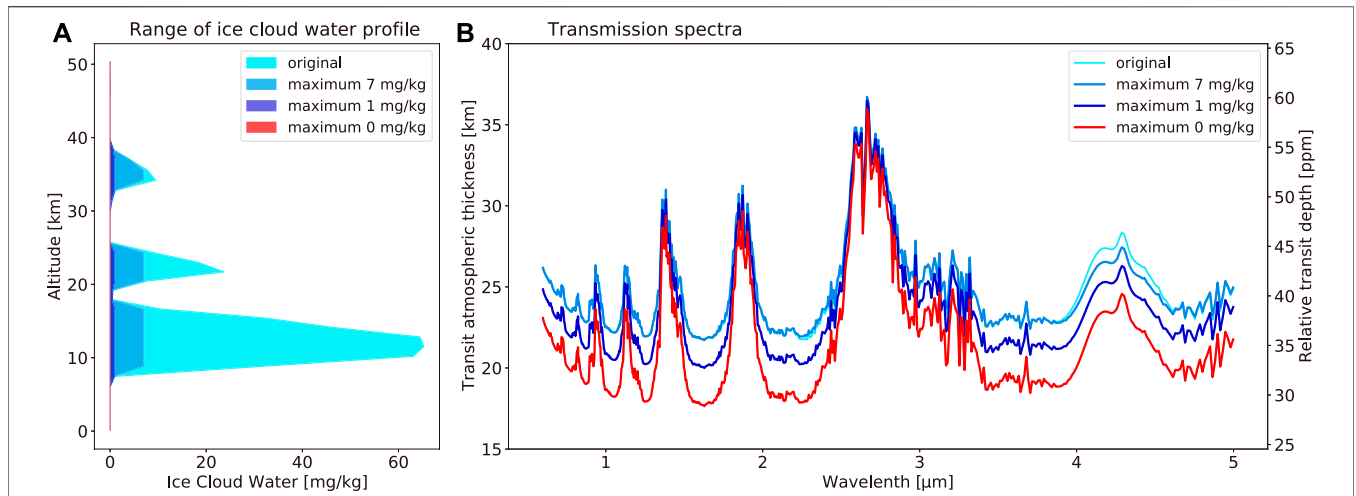


FIGURE 7 | The saturation effect of ice cloud water on transmission thickness in the rapidly rotating case of six Earth days. The shadings in (A) show the range of ice cloud water content along the morning terminator. We artificially set the maximum value of ice cloud water to 0, 1, and 7 mg kg⁻¹ in (A), and their corresponding transit atmospheric thicknesses are shown in (B). When the maximum value of ice cloud water is set to 7 mg kg⁻¹, the transit atmospheric thickness is almost the same as the original, and we call this phenomenon “the saturation effect”.

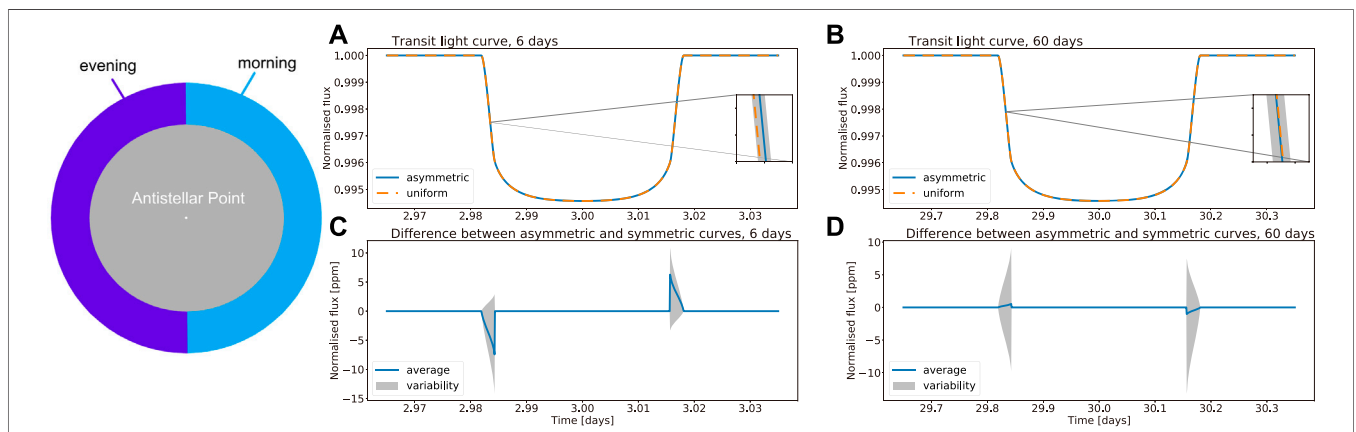


FIGURE 8 | Light curves of primary transit for the real case (blue color) and an imagined symmetric planet (orange color). Panels (A) and (C) show the results for planets with a rotation period of six Earth days. Panels (B) and (D) show the results for planets with a rotation period of 60 Earth days. The lines are the mean values and the gray shading represents the variability. (C) and (D) are for the differences between the real case and the imagined symmetric planet. The light curves were calculated using the module PyTransit, a fast exoplanet transit model written in Python (Parviainen, 2015), and the light curves are summed over 0.6–5 μm, the same as the spectral range of transmission spectra in Figure 2.

period, it needs more than 300 transits to achieve 3σ detection, which is impossible during the lifetime of the JWST. In these calculations of the transit number, the variability was not considered; if it is included, the transit number would be at least doubled for a planet with a rotation period of six Earth days, since the 20 ppm variability is a bit larger than the output of PSG’s noise calculator, which is about 15 ppm. The updated estimation is 55 transits to reach 3σ detection, and 150 transits to reach 5σ detection for the rapidly rotating case.

The asymmetry and variability are also reflected in the transit light curve, especially for the rapidly rotating case. Figures 8A,B show the shape of the light curves of the real case and an imagined symmetric planet. In this study, we use the module of PyTransit

(Parviainen, 2015) to calculate the transit light curves. The basic principle is summarized here: considering an orbit without inclination, the normalized total flux *f* during the transit is as follows:

$$f(d) = 1 - \frac{1}{\pi} \left[\left(\frac{r}{R} \right)^2 \kappa_1 + \kappa_2 - \sqrt{\frac{d^2}{R^2} - \frac{(R^2 + d^2 - r^2)^2}{4R^4}} \right], \quad (2)$$

where $\kappa_1 = \arccos\left(\frac{r^2 + d^2 - R^2}{2rd}\right)$ and $\kappa_2 = \arccos\left(\frac{R^2 + d^2 - r^2}{2Rd}\right)$ (Mandel and Agol, 2002). *R* is the stellar radius, *r* is the radius of the planet, and *d* is the center-to-center distance between the star and the planet from front view, as shown in Figure 1B in Mandel and Agol (2002). We set *R* the same as TRAPPIST-1, and

assume that there is no inclination of the orbit. During the ingress, $r = r_0 + AT_{\text{morning}}$, and during the egress, $r = r_0 + AT_{\text{evening}}$, where r_0 is the radius of TRAPPIST-1e, and AT is the transit atmospheric thickness. The effect of limb darkening (i.e., the limb of the star appears darker than the center of the star) is considered using the method of Mandel and Agol (2002) and de Wit et al. (2016).

The asymmetry in the spatial patterns of clouds and water vapor results in a distortion of the light curve. The distortion for the rapidly rotating planet is larger than that for the slowly rotating planet, similar to the results in the transmission spectra. The distortion implies a late transit, but the timing offset is in the order of one second. The small magnitude of the offset, in addition to the confusing effect of the large variability (Figures 8C,D), makes it very difficult to be detected in the observations of the JWST.

4 SUMMARY AND DISCUSSION

In this study, we use PSG to calculate the transmission spectra of 1:1 tidally locked planets, based on the climatic states simulated using 3D global atmospheric circulation simulations. We focus on two important aspects that were not seriously considered in previous studies: the asymmetry between the morning and evening terminators and the variability of the transmission spectra. We find that there is significant asymmetry in the transmission spectra between the morning and evening terminators, especially for rapidly rotating planets. Ice clouds contribute the most to the asymmetry, due to the fact that they are at high levels, thus having a longer optical path. For rapidly rotating planets, the asymmetry is mainly caused by coupled Rossby–Kelvin waves and equatorial superrotation that transport water vapor and clouds to the evening terminator from the substellar region. Moreover, there is strong variability in the transmission spectra for both morning and evening terminators and for both rapidly and slowly rotating planets. This variability makes the detection of the asymmetry by the JWST almost impossible.

In calculating the transit atmospheric thickness, shown in Figure 2 and Figure 8, we set both cases to have the same stellar radius, the radius of a 2600 K star. However, in reality, a star of 3700 K should have a radius three to four times of a 2600 K star. For example, the radius of TRAPPIST-1 with stellar temperature of $2,516 \pm 41$ K is about 0.12 solar radius (Van Grootel et al., 2018), and the radius of Gliese 667 C, whose stellar temperature is $3,700 \pm 100$ K (Anglada-Escudé et al., 2012), is 0.42 solar radius. Considering the increment of stellar radius, the relative transit depth of the slowly rotating planet would be decreased by 10–20 times, so it is even more impossible to detect the asymmetry on a slowly rotating planet.

We only include N_2 and H_2O in this study. The atmospheric composition is simple and the planet is under a fixed stellar flux. If other species, such as O_3 , which exists above the ice cloud deck, were considered in the simulations, the asymmetry might be even larger. If continents were included, the asymmetry may increase or decrease, depending on the location of the continents and the complex interactions among land, atmosphere, and clouds. In Zhang and Yang (2020), climatic states under different atmospheric pressures

(from 0.5 to 4.0 bar) and stellar fluxes (from 1,200 to 1800 W m^{-2}) had also been simulated. When using these climatic outputs to calculate the transmission spectra, we found that the magnitude of the asymmetry in all the experiments are between the rapidly rotating case and the slowly rotating case shown in section 3, and no clear trend of the transmission spectra as a function of the air pressure or stellar flux was found (figures not shown). We have also calculated the effect of oceanic heat transport on the magnitude of the asymmetry using the climatic outputs of coupled atmosphere–ocean general circulation experiments done in Yang et al. (2019a). We found that oceanic heat transport has a small effect (less than 3 ppm) on the asymmetry amplitude and the effect is negative under rapidly rotating orbits but positive under slowly rotating orbits (figures not shown).

Espinoza and Jones (2021) presented a semi-analytical framework to extract the transmission spectra of the morning terminator and the evening terminator directly from transit light curves and showed that current missions like the JWST and TESS are capable of detecting the asymmetry signal larger than 25 ppm. As shown in Figure 7 of their study, the method is effective for hot Jupiters. For terrestrial planets, it will be more difficult, since the planet-to-star radius ratio and the asymmetry signal of terrestrial planets are smaller than those of hot Jupiters. Future larger telescopes with higher precisions will be more likely to detect the asymmetry signals between morning and evening terminators of habitable terrestrial planets.

Finally, we mention that the transmission spectra highly depend on the ice clouds at and around the terminators, but both convection and clouds in these models are parameterized based on the understandings of Earth. Because the scale of clouds is always smaller than the model grid sizes of GCMs, cloud water path, and cloud fraction are parameterized. Different GCMs use different cloud parameterization schemes. Previous model intercomparisons for tidally locked habitable planets have shown that there are large differences in simulated cloud water path and cloud fraction between GCMs (Fauchez T. et al., 2019; Yang et al., 2019b). Many processes and parameters in the models can influence the simulation results. For example, the partition between liquid cloud and ice cloud is always parameterized based on air temperature in the microphysics modules. In ExoCAM, the fraction of cloud ice water in total condensate is set to be 100% when air temperature is lower than -40°C and to be 0% when the air temperature is higher than -10°C ; between -40°C and -10°C , the fraction of cloud ice water is a linear function of the air temperature (Collins et al., 2004). In the model SAM, a similar linear function is used but the two temperature limits are set to be -20°C and 0°C (Khairoutdinov and Randall, 2003). For the latter, the cloud ice water path will be higher and the transmission thickness will be larger, if under the same condition. Another example is that the particle size of ice clouds is also parameterized in GCMs. In real world, the particle size as well as terminal velocity is determined by microphysical processes and should depend on air mass and planetary gravity (Loftus and Wordsworth, 2021), but this mechanism has not been included in present GCMs yet. In future studies, cloud-resolving experiments with explicit convection and clouds are required to provide more confident conclusions.

DATA AVAILABILITY STATEMENT

The original contributions presented in the study are included in the article; further inquiries can be directed to the corresponding author.

AUTHOR CONTRIBUTIONS

JY formulated the problem and designed the experiments. XS calculated the spectra, analyzed the data, and drew the figures. Both authors discussed the results and wrote the manuscript.

REFERENCES

- Allard, F., Allard, N. F., Homeier, D., Kielkopf, J., McCaughrean, M. J., and Spiegelman, F. (2007). K-H2 Quasi-Molecular Absorption Detected in the T-dwarf Indi Ba. *A&A* 474, L21–L24. doi:10.1051/0004-6361:20078362
- Anglada-Escudé, G., Arriagada, P., Vogt, S. S., Rivera, E. J., Butler, R. P., Crane, J. D., et al. (2012). A Planetary System Around the Nearby M dwarf GJ 667C with at Least One Super-earth in its Habitable Zone. *ApJ* 751, L16. doi:10.1088/2041-8205/751/1/L16
- Apai, D., Radigan, J., Buenzli, E., Burrows, A., Reid, I. N., and Jayawardhana, R. (2013). HstSpectral Mapping of L/T Transition Brown Dwarfs Reveals Cloud Thickness Variations. *ApJ* 768, 121. doi:10.1088/0004-637x/768/2/121
- Artigau, É., Bouchard, S., Doyon, R., and Lafrenière, D. (2009). Photometric Variability of the T2.5 Brown dwarf SIMP J013656.5+093347: Evidence for Evolving Weather Patterns. *ApJ* 701, 1534–1539. doi:10.1088/0004-637x/701/2/1534
- Barnes, R. (2017). Tidal Locking of Habitable Exoplanets. *Celest. Mech. Dyn. Astr.* 129, 509–536. doi:10.1007/s10569-017-9783-7
- Batalha, N. E., Lewis, N. K., Line, M. R., Valenti, J., and Stevenson, K. (2018). Strategies for Constraining the Atmospheres of Temperate Terrestrial Planets with JWST. *ApJ* 856, L34. doi:10.3847/2041-8213/aab896
- Benneke, B., Wong, I., Piaulet, C., Knutson, H. A., Lothringer, J., Morley, C. V., et al. (2019). Water Vapor and Clouds on the Habitable-Zone Sub-Neptune Exoplanet K2-18b. *ApJ* 887, L14. doi:10.3847/2041-8213/ab59dc
- Bin, J., Tian, F., and Liu, L. (2018). New Inner Boundaries of the Habitable Zones Around M Dwarfs. *Earth Planet. Sci. Lett.* 492, 121–129. doi:10.1016/j.epsl.2018.04.003
- Charbonneau, D., Brown, T. M., Noyes, R. W., and Gilliland, R. L. (2002). Detection of an Extrasolar Planet Atmosphere. *ApJ* 568, 377–384. doi:10.1086/338770
- Charnay, B., Blain, D., Bézard, B., Leconte, J., Turbet, M., and Falco, A. (2021). Formation and Dynamics of Water Clouds on Temperate Sub-neptunes: the Example of K2-18b. *A&A* 646, A171. doi:10.1051/0004-6361/202039525
- Collins, W. D., Rasch, P. J., Boville, B. A., Hack, J. J., McCaa, J. R., Williamson, D. L., et al. (2004). *Description of the NCAR Community Atmosphere Model (CAM 3.0)*. (No. NCAR/TN-464+STR). Boulder, CO: University Corporation for Atmospheric Research. doi:10.5065/D63N21CH
- de Wit, J., Wakeford, H. R., Gillon, M., Lewis, N. K., Valenti, J. A., Demory, B.-O., et al. (2016). A Combined Transmission Spectrum of the Earth-Sized Exoplanets TRAPPIST-1 B and C. *Nature* 537, 69–72. doi:10.1038/nature18641
- de Wit, J., Wakeford, H. R., Lewis, N. K., Delrez, L., Gillon, M., Selsis, F., et al. (2018). Atmospheric Reconnaissance of the Habitable-Zone Earth-Sized Planets Orbiting TRAPPIST-1. *Nat. Astron.* 2, 214–219. doi:10.1038/s41550-017-0374-z
- Deming, L. D., and Seager, S. (2017). Illusion and Reality in the Atmospheres of Exoplanets. *J. Geophys. Res. Planets* 122, 53–75. doi:10.1002/2016je005155
- Dobbs-Dixon, I., Agol, E., and Burrows, A. (2012). The Impact of Circumplanetary Jets on Transit Spectra and Timing Offsets for Hot Jupiters. *ApJ* 751, 87. doi:10.1088/0004-637x/751/2/87
- Ehrenreich, D., Lovis, C., Allart, R., Zapatero Osorio, M. R., Pepe, F., Cristiani, S., et al. (2020). Nightside Condensation of Iron in an Ultrahot Giant Exoplanet. *Nature* 580, 597–601. doi:10.1038/s41586-020-2107-1
- Espinoza, N., and Jones, K. (2021). *Constraining Mornings & Evenings on Distant Worlds: A New Semi-analytical Approach and Prospects with Transmission Spectroscopy*. *arXiv preprint arXiv:2106.15687*.

FUNDING

JY acknowledges support from the National Natural Science Foundation of China (NSFC) under grant 41888101 and 42075046.

ACKNOWLEDGMENTS

We thank Eric Wolf for the release of ExoCAM and thank NASA for the release of PSG. We are grateful to the help from Yixiao Zhang, Thaddeus D. Komacek, Xi Zhang, and Guo Chen.

- Faucher, T. J., Turbet, M., Villanueva, G. L., Wolf, E. T., Arney, G., Kopparapu, R. K., et al. (2019b). Impact of Clouds and Hazes on the Simulated JWST Transmission Spectra of Habitable Zone Planets in the TRAPPIST-1 System. *ApJ* 887, 194. doi:10.3847/1538-4357/ab5862
- Faucher, T., Turbet, M., Wolf, E. T., Boutle, I., Way, M. J., Del, A. D., et al. (2019a). TRAPPIST-1 Habitable Atmosphere Intercomparison (Thai). Motivations and Protocol. *Geoscientific Model. Dev. Discuss.* 2019, 1–15. doi:10.5194/gmd-13-707-2020
- Grimm, S. L., Demory, B.-O., Gillon, M., Dorn, C., Agol, E., Burdanov, A., et al. (2018). The Nature of the TRAPPIST-1 Exoplanets. *A&A* 613, A68. doi:10.1051/0004-6361/201732233
- Groot, V. V., Fernandes, C. S., Gillon, M., Jehin, E., Manfroid, J., Scaiffare, R., et al. (2018). Stellar Parameters for TRAPPIST-1. *ApJ* 853, 30. doi:10.3847/1538-4357/aaa023
- Hammond, M., and Pierrehumbert, R. T. (2018). Wave-mean Flow Interactions in the Atmospheric Circulation of Tidally Locked Planets. *ApJ* 869, 65. doi:10.3847/1538-4357/aaec03
- Haqq-Misra, J., Wolf, E. T., Joshi, M., Zhang, X., and Kopparapu, R. K. (2018). Demarcating Circulation Regimes of Synchronously Rotating Terrestrial Planets within the Habitable Zone. *ApJ* 852, 67. doi:10.3847/1538-4357/aa9f1f
- Hubbard, W. B., Fortney, J. J., Lunine, J. I., Burrows, A., Sudarsky, D., and Pinto, P. (2001). Theory of Extrasolar Giant Planet Transits. *ApJ* 560, 413–419. doi:10.1086/322490
- Iyer, A. R., and Line, M. R. (2020). The Influence of Stellar Contamination on the Interpretation of Near-Infrared Transmission Spectra of Sub-Neptune Worlds Around M-Dwarfs. *ApJ* 889, 78. doi:10.3847/1538-4357/ab612e
- Kaltenegger, L. (2017). How to Characterize Habitable Worlds and Signs of Life. *Annu. Rev. Astron. Astrophys.* 55, 433–485. doi:10.1146/annurev-astro-082214-122238
- Kasting, J. F., Whitmire, D. P., and Reynolds, R. T. (1993). Habitable Zones Around Main Sequence Stars. *Icarus* 101, 108–128. doi:10.1006/icar.1993.1010
- Kesseli, A. Y., and Snellen, I. A. G. (2021). Confirmation of Asymmetric Iron Absorption in WASP-76b with HARPS. *ApJ* 908, L17. doi:10.3847/2041-8213/abe047
- Kopparapu, R. k., Wolf, E. T., Arney, G., Batalha, N. E., Haqq-Misra, J., Grimm, S. L., et al. (2017). Habitable Moist Atmospheres on Terrestrial Planets Near the Inner Edge of the Habitable Zone Around M Dwarfs. *ApJ* 845, 5. doi:10.3847/1538-4357/aa7cf9
- Kopparapu, R. k., Wolf, E. T., Haqq-Misra, J., Yang, J., Kasting, J. F., Meadows, V., et al. (2016). The Inner Edge of the Habitable Zone for Synchronously Rotating Planets Around Low-Mass Stars Using General Circulation Models. *ApJ* 819, 84. doi:10.3847/0004-637x/819/1/84
- Kreidberg, L. (2017). “Exoplanet Atmosphere Measurements from Transmission Spectroscopy and Other Planet star Combined Light Observations,” in *Handbook of Exoplanets* (Springer International Publishing), 1–23. doi:10.1007/978-3-319-30648-3_100-1
- Lacy, B. L., and Burrows, A. (2020). JWST Transit Spectra. I. Exploring Potential Biases and Opportunities in Retrievals of Tidally Locked Hot Jupiters with Clouds and Hazes. *ApJ* 905, 131. doi:10.3847/1538-4357/abc01c
- Lincowski, A. P., Lustig-Yaeger, J., and Meadows, V. S. (2019). Observing Isotopologue Bands in Terrestrial Exoplanet Atmospheres with the James Webb Space Telescope: Implications for Identifying Past Atmospheric and Ocean Loss. *Aj* 158, 26. doi:10.3847/1538-3881/ab2385
- Lincowski, A. P., Meadows, V. S., Crisp, D., Robinson, T. D., Luger, R., Lustig-Yaeger, J., et al. (2018). Evolved Climates and Observational Discriminants for the TRAPPIST-1 Planetary System. *ApJ* 867, 76. doi:10.3847/1538-4357/aae36a
- Line, M. R., and Parmentier, V. (2016). The Influence of Nonuniform Cloud Cover on Transit Transmission Spectra. *ApJ* 820, 78. doi:10.3847/0004-637x/820/1/78

- Loftus, K., and Wordsworth, R. D. (2021). The Physics of Falling Raindrops in Diverse Planetary Atmospheres. *J. Geophys. Res. Planets* 126, e2020JE006653. doi:10.1029/2020je006653
- Lustig-Yaeger, J., Meadows, V. S., and Lincowski, A. P. (2019). The Detectability and Characterization of the TRAPPIST-1 Exoplanet Atmospheres with JWST. *Aj* 158, 27. doi:10.3847/1538-3881/ab21e0
- Mandel, K., and Agol, E. (2002). Analytic Light Curves for Planetary Transit Searches. *Astrophysical J. Lett.* 580, L171–L175. doi:10.1086/345520
- May, E. M., Taylor, J., Komacek, T. D., Line, M. R., and Parmentier, V. (2021). Water Ice Cloud Variability and Multi-epoch Transmission Spectra of TRAPPIST-1e. *ApJL* 911, L30. doi:10.3847/2041-8213/abefff
- Mayor, M., and Queloz, D. (1995). A Jupiter-mass Companion to a Solar-type star. *Nature* 378, 355–359. doi:10.1038/378355a0
- Merlis, T. M., and Schneider, T. (2010). Atmospheric Dynamics of Earth-like Tidally Locked Aquaplanets. *J. Adv. Model. Earth Syst.* 2. doi:10.3894/james.2010.2.13
- Mikal-Evans, T., Crossfield, I. J. M., Benneke, B., Kreidberg, L., Moses, J., Morley, C. V., et al. (2020). Transmission Spectroscopy for the Warm Sub-Neptune HD 3167c: Evidence for Molecular Absorption and a Possible High-Metallicity Atmosphere. *Aj* 161, 18. doi:10.3847/1538-3881/abc874
- Nikolov, N., Sing, D. K., Pont, F., Burrows, A. S., Fortney, J. J., Ballester, G. E., et al. (2014). Hubble Space Telescope Hot Jupiter Transmission Spectral Survey: a Detection of Na and strong Optical Absorption in HAT-P-1b. *Monthly Notices R. Astronomical Soc.* 437, 46–66. doi:10.1093/mnras/stt1859
- Noda, S., Ishiwatari, M., Nakajima, K., Takahashi, Y. O., Takehiro, S., Onishi, M., et al. (2017). The Circulation Pattern and Day-Night Heat Transport in the Atmosphere of a Synchronously Rotating Aquaplanet: Dependence on Planetary Rotation Rate. *Icarus* 282, 1–18. doi:10.1016/j.icarus.2016.09.004
- Parmentier, V., Line, M. R., Bean, J. L., Mansfield, M., Kreidberg, L., Lupu, R., et al. (2018). From thermal Dissociation to Condensation in the Atmospheres of Ultra Hot Jupiters: WASP-121b in Context. *A&A* 617, A110. doi:10.1051/0004-6361/201833059
- Parviainen, H. (2015). PYTRANSIT: Fast and Easy Exoplanet Transit Modelling in PYTHON. *Monthly Notices R. Astronomical Soc.* 450, 3233–3238. doi:10.1093/mnras/stv894
- Pidhorodetska, D., Fauchez, T. J., Villanueva, G. L., Domagal-Goldman, S. D., and Kopparapu, R. K. (2020). Detectability of Molecular Signatures on TRAPPIST-1e through Transmission Spectroscopy Simulated for Future Space-based Observatories. *ApJ* 898, L33. doi:10.3847/2041-8213/aba4a1
- Pierrehumbert, R. T., and Hammond, M. (2019). Atmospheric Circulation of Tide-Locked Exoplanets. *Annu. Rev. Fluid Mech.* 51, 275–303. doi:10.1146/annurev-fluid-010518-040516
- Pluriel, W., Zingales, T., Leconte, J., and Parmentier, V. (2020). Strong Biases in Retrieved Atmospheric Composition Caused by Day-Night Chemical Heterogeneities. *A&A* 636, A66. doi:10.1051/0004-6361/202037678
- Powell, D., Louden, T., Kreidberg, L., Zhang, X., Gao, P., and Parmentier, V. (2019). Transit Signatures of Inhomogeneous Clouds on Hot Jupiters: Insights from Microphysical Cloud Modeling. *ApJ* 887, 170. doi:10.3847/1538-4357/ab55d9
- Radigan, J., Jayawardhana, R., Lafrenière, D., Artigau, É., Marley, M., and Saumon, D. (2012). Large-amplitude Variations of an L/T Transition Brown dwarf: Multi-Wavelength Observations of Patchy, High-Contrast Cloud Features. *ApJ* 750, 105. doi:10.1088/0004-637x/750/2/105
- Schwieterman, E. W., Kiang, N. Y., Parenteau, M. N., Harman, C. E., DasSarma, S., Fisher, T. M., et al. (2018). Exoplanet Biosignatures: a Review of Remotely Detectable Signs of Life. *Astrobiology* 18, 663–708. doi:10.1089/ast.2017.1729
- Seager, S., and Sasselov, D. D. (2000). Theoretical Transmission Spectra during Extrasolar Giant Planet Transits. *ApJ* 537, 916–921. doi:10.1086/309088
- Showman, A. P., and Polvani, L. M. (2011). Equatorial Superrotation on Tidally Locked Exoplanets. *ApJ* 738, 71. doi:10.1088/0004-637x/738/1/71
- Showman, A. P., and Polvani, L. M. (2010). The Matsuno-Gill Model and Equatorial Superrotation. *Geophys. Res. Lett.* 37, a–n. doi:10.1029/2010gl044343
- Showman, A. P., Tan, X., and Zhang, X. (2019). Atmospheric Circulation of Brown Dwarfs and Jupiter- and Saturn-like Planets: Zonal Jets, Long-Term Variability, and QBO-type Oscillations. *ApJ* 883, 4. doi:10.3847/1538-4357/ab384a
- Showman, A. P., Wordsworth, R. D., Merlis, T. M., and Kaspi, Y. (2013). Atmospheric Circulation of Terrestrial Exoplanets. *Comp. Climatology Terrestrial Planets* 1, 277–326. doi:10.2458/azu_uapress_9780816530595-ch12
- Sing, D. K., Désert, J.-M., Fortney, J. J., Lecavelier des Etangs, A., Ballester, G. E., Cepa, J., et al. (2011). Gran Telescopio Canarias OSIRIS Transiting Exoplanet Atmospheric Survey: Detection of Potassium in XO-2b from Narrowband Spectrophotometry. *A&A* 527, A73. doi:10.1051/0004-6361/201015579
- Snellen, I. A. G., Désert, J.-M., Waters, L. B. F. M., Robinson, T., Meadows, V., van Dishoeck, E. F., et al. (2017). Detecting Proxima B's Atmosphere with JWST Targeting CO₂ at 15 μ m Using a High-Pass Spectral Filtering Technique. *Aj* 154, 77. doi:10.3847/1538-3881/aa7fbc
- Suissa, G., Mandell, A. M., Wolf, E. T., Villanueva, G. L., Fauchez, T., and Kopparapu, R. K. (2020a). Dim Prospects for Transmission Spectra of Ocean Earths Around M Stars. *ApJ* 891, 58. doi:10.3847/1538-4357/ab72f9
- Suissa, G., Wolf, E. T., Kopparapu, R. K., Villanueva, G. L., Fauchez, T., Mandell, A. M., et al. (2020b). The First Habitable-Zone Earth-Sized Planet from TESS. III. Climate States and Characterization Prospects for TOI-700 D. *Aj* 160, 118. doi:10.3847/1538-3881/aba4b4
- Tsai, S.-M., Dobbs-Dixon, I., and Gu, P.-G. (2014). Three-dimensional Structures of Equatorial Waves and the Resulting Super-rotation in the Atmosphere of a Tidally Locked Hot Jupiter. *ApJ* 793, 141. doi:10.1088/0004-637x/793/2/141
- Vallis, G. K. (2006). *Atmospheric and Oceanic Fluid Dynamics*. Cambridge University Press. doi:10.1017/cbo9780511790447
- Villanueva, G. L., Smith, M. D., Protopapa, S., Faggi, S., and Mandell, A. M. (2018). Planetary Spectrum Generator: An Accurate Online Radiative Transfer Suite for Atmospheres, Comets, Small Bodies and Exoplanets. *J. Quantitative Spectrosc. Radiative Transfer* 217, 86–104. doi:10.1016/j.jqsrt.2018.05.023
- von Paris, P., Gratier, P., Bordé, P., Leconte, J., and Selsis, F. (2016). Inferring Asymmetric Limb Cloudiness on Exoplanets from Transit Light Curves. *A&A* 589, A52. doi:10.1051/0004-6361/201527894
- Wakeford, H. R., and Sing, D. K. (2015). Transmission Spectral Properties of Clouds for Hot Jupiter Exoplanets. *A&A* 573, A122. doi:10.1051/0004-6361/201424207
- Wang, S., and Yang, J. (2021). Phase Shift of Planetary Waves and Wave-Jet Resonance on Tidally Locked Planets. *ApJ* 907, 28. doi:10.3847/1538-4357/abcf2a
- Way, M. J., Del Genio, A. D., Kiang, N. Y., Sohl, L. E., Grinspoon, D. H., Aleinov, I., et al. (2016). Was Venus the First Habitable World of Our Solar System? *Geophys. Res. Lett.* 43, 8376–8383. doi:10.1002/2016gl069790
- Winn, J. N. (2010). Exoplanet Transits and Occultations. *Exoplanets* 1, 55–77.
- Wolf, E. T. (2017). Assessing the Habitability of the TRAPPIST-1 System Using a 3D Climate Model. *ApJ* 839, L1. doi:10.3847/2041-8213/aa693a
- Wolf, E. T., Shields, A. L., Kopparapu, R. K., Haqq-Misra, J., and Toon, O. B. (2017). Constraints on Climate and Habitability for Earth-like Exoplanets Determined from a General Circulation Model. *ApJ* 837, 107. doi:10.3847/1538-4357/aa5ffc
- Wolf, E. T., and Toon, O. B. (2014). Controls on the Archaean Climate System Investigated with a Global Climate Model. *Astrobiology* 14, 241–253. doi:10.1089/ast.2013.1112
- Yang, J., Abbot, D. S., Koll, D. D. B., Hu, Y., and Showman, A. P. (2019a). Ocean Dynamics and the Inner Edge of the Habitable Zone for Tidally Locked Terrestrial Planets. *ApJ* 871, 29. doi:10.3847/1538-4357/aaf1a8
- Yang, J., Cowan, N. B., and Abbot, D. S. (2013). Stabilizing Cloud Feedback Dramatically Expands the Habitable Zone of Tidally Locked Planets. *ApJ* 771, L45. doi:10.1088/2041-8205/771/2/L45
- Yang, J., Leconte, J., Wolf, E. T., Merlis, T., Koll, D. D. B., Forget, F., et al. (2019b). Simulations of Water Vapor and Clouds on Rapidly Rotating and Tidally Locked Planets: A 3D Model Intercomparison. *ApJ* 875, 46. doi:10.3847/1538-4357/ab09f1
- Zhang, Y., and Yang, J. (2020). How Does Background Air Pressure Influence the Inner Edge of the Habitable Zone for Tidally Locked Planets in a 3D View? *ApJ* 901, L36. doi:10.3847/2041-8213/abb87f

Conflict of Interest: The authors declare that the research was conducted in the absence of any commercial or financial relationships that could be construed as a potential conflict of interest.

Publisher's Note: All claims expressed in this article are solely those of the authors and do not necessarily represent those of their affiliated organizations, or those of the publisher, the editors, and the reviewers. Any product that may be evaluated in this article, or claim that may be made by its manufacturer, is not guaranteed or endorsed by the publisher.

Copyright © 2021 Song and Yang. This is an open-access article distributed under the terms of the Creative Commons Attribution License (CC BY). The use, distribution or reproduction in other forums is permitted, provided the original author(s) and the copyright owner(s) are credited and that the original publication in this journal is cited, in accordance with accepted academic practice. No use, distribution or reproduction is permitted which does not comply with these terms.